

Electronic Supplementary Information

Unique tetranuclear Ag(I) complex emitting efficient thermally activated delayed fluorescence with a remarkably short decay time

Xue-Min Gan,^{ab} Rongmin Yu,^{*a} Xu-Lin Chen,^a MingXue Yang,^{ab} Ling Lin,^{ab} Xiao-Yuan Wu,^a and Can-Zhong Lu^{*a}

a Key Laboratory of Design and Assembly of Functional Nanostructures, Fujian Provincial Key Laboratory of Nanomaterials, Fujian Institute of Research on the Structure of Matter, Chinese Academy of Sciences.

*E-mail: czlu@fjirsm.ac.cn

b Graduate University of Chinese Academy of Sciences, Beijing 100049, China

Contents

1. General procedures.

2. Synthesis and characterization.

Fig. S1 Synthesis of the ligand: DMPTPH.

Fig. S2 Synthesis of the complex: Ag₄N₂P₃.

Fig. S3 Powder X-ray diffraction (PXRD) patterns for Ag₄N₂P₃.

Fig. S4 TGA-plots for Ag₄N₂P₃.

3. Crystal Structure Determination.

Table S1. Crystallographic data for complex Ag₄N₂P₃.

Table S2. Selected bond distances (Å) and angles (°) of complex Ag₄N₂P₃.

Fig. S5 ORTEP diagram of Ag₄N₂P₃

Fig. S6 The structure presentation of Ag₄N₂P₃

Fig. S7 Schematic representation of the geometrical parameters θ in Ag₄N₂P₃ viewed from different sides.

4. Computational studies

Table S3. The partition orbital composition analyses for the frontier molecular orbitals of complex Ag₄N₂P₃.

Fig. S8 The frontier orbitals from HOMO-5 to LUMO+2 of complex Ag₄N₂P₃ (based on the X-ray structure).

Table S4. Orbital transition analyses for lower-lying transition of complex Ag₄N₂P₃.

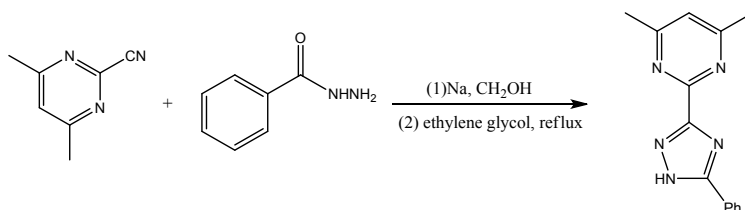
Table S5. The partition composition analyses for the lower-lying excited states of complex Ag₄N₂P₃.

1. General procedures.

All reagents are available from commercial sources and were used as received without purification or drying. ^1H spectra were recorded on a Bruker Avance III 400 MHz NMR spectrometer. Elemental analyses (C, H, N) were carried out using an Elemental Vario EL III elemental analyzer. Powder X-ray diffraction (PXRD) were collected on Rigaku desktop MiniFlex 600 diffractometer with Cu $K\alpha$ radiation ($\lambda=1.5418 \text{ \AA}$). IR spectra were recorded in the range 4000–400 cm^{-1} on a Perkin-Elmer FTIR spectrum 2000 spectrometer with pressed KBr pellets. Thermal analyses were performed on a TGA/DSC 1 STARe system from room temperature to 800 $^\circ\text{C}$ with a heating rate of 10 K/min under nitrogen. The UV-vis absorption spectra were recorded using a Perkin-Elmer Lambda-365 UV/vis spectrophotometer. Photoluminescence spectra for solid samples at both 298 K and 77 K were recorded on a HORIBA Jobin-Yvon FluoroMax-4 SPECTROMETER. The lifetimes at different temperatures were determined using a HORIBA Jobin-Yvon FluoroMax-4 instrument with multi-channel scaling (MCS). Emission decay data were analyzed by using the software DAS6 (time-correlated single-photon counting Decay Analysis Software) peripheral equipment. The PL quantum yields measurements of the solids and films equipped with HORIBA Jobin-Yvon FluoroMax-4-equipped with an integrating sphere.

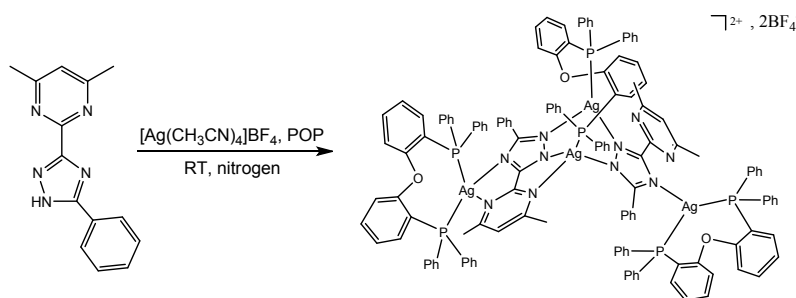
2. Experimental Section.

Fig. S1 Synthesis of the ligand: 2-bromo-6-(3-phenyl-1H-pyrazol-1-yl)pyridine (DMPTPH).



To a stirred suspension of 4,6-dimethylpyrimidine-2-carbonitrile (0.666 g, 5 mmol) in distilled methanol (8 mL) was added sodium (0.230 g, 10 mmol) under nitrogen. After ten minutes, benzohydrazide (0.681 g, 5 mmol) was added and stirred for 30 min at room temperature. The reaction mixture was refluxed overnight to form a large amount of yellow precipitate. After cooling the mixture was filtered and washed with methanol. After being dried for one day, the solid was mixed with 3 ml ethyleneglycol and heated at 200 $^\circ\text{C}$ for 2 h. After cooling to room temperature, the reaction mixture subsequently quenched with 30 ml of water. The aqueous layer was extracted with 3 \times 30 mL dichloromethane. Afterward the organic layers were combined, washed with 50 mL brine, and dried over anhydrous Na_2SO_4 . The crude product was purified by column chromatography on silica gel and dried under vacuum to afford a white solid (1.043 g, 83%). ^1H NMR (400 MHz, DMSO- d_6): δ 14.90 (s, 1H), 8.11 (d, J = 7.6 Hz, 2H), 7.60 – 7.42 (m, 3H), 7.39 (s, 1H), 2.55 (s, 6H).

Fig. S2 Synthesis of the complex: $[\text{Ag}_4(\mu\text{-DMPTP})_2(\text{POP})_3][\text{BF}_4]_2$ ($\text{Ag}_4\text{N}_2\text{P}_3$).



A mixture of 2-bromo-6-(3-phenyl-1H-pyrazol-1-yl)pyridine (DMPTPH) (0.050 g, 0.2 mmol), $[\text{Ag}(\text{CH}_3\text{CN})_4]\text{BF}_4$ (0.143 g, 0.4 mmol) in dry dichloromethane (10 mL) under a nitrogen atmosphere was stirred for 0.5 h and then bis[2-(diphenylphosphine)phenyl]ether (POP) (0.016 g, 0.3 mmol) was added. After stirring for another 3 h, the solvent was evaporated. Yield: 137 mg, 52%. Single crystals of these products suitable for X-ray diffraction measurements were obtained by low evaporation of its mixed solvent of dichloromethane and ethanol ($v:v = 2:1$).

$[\text{Ag}_4(\mu\text{-DMPTP})_2(\text{POP})_3][\text{BF}_4]_2$. FTIR (KBr pellet, cm^{-1}): 3056m, 1635w, 1593s, 1562w, 1540s, 1462s, 1435s, 1386w, 1350w, 1260s, 1218s, 1160w, 1055s, 871w, 801w, 748s, 694s, 510s, 473s. Anal. calcd for $\text{C}_{142}\text{H}_{126}\text{Ag}_4\text{N}_{10}\text{P}_6\text{B}_2\text{F}_8\text{O}_6$: C, 59.63; H, 4.41; N, 4.89. Found: C, 59.89; H, 4.09; N, 4.75.

Fig. S3 Powder X-ray diffraction (PXRD) patterns for $\text{Ag}_4\text{N}_2\text{P}_3$.

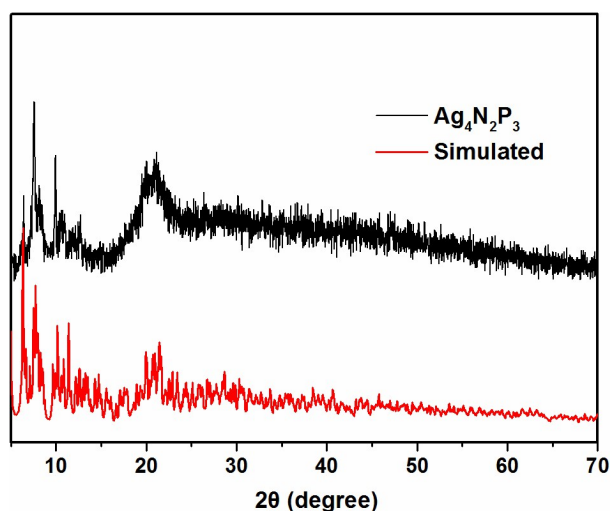
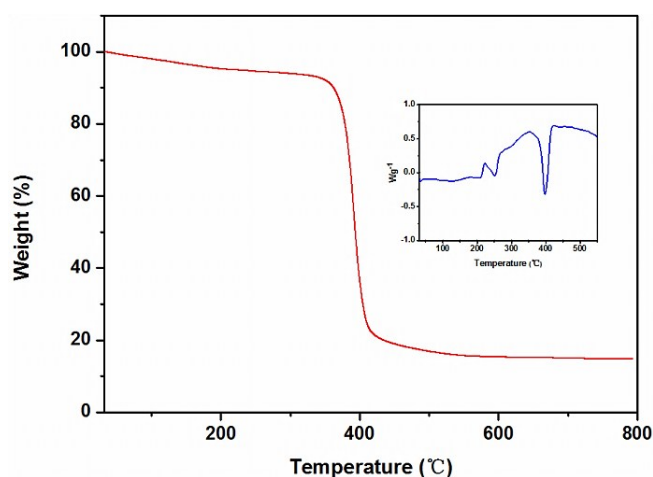


Fig. S4 TGA and DSC plots for $\text{Ag}_4\text{N}_2\text{P}_3$.



3. Crystal Structure Determination.

Crystallographic data for the complexes were mounted on loop for the X-ray measurement. Diffraction data

collected on a SuperNova, Dual source, Cu at zero, Atlas diffractometer equipped with graphic monochromated Cu K α radiation ($\lambda=1.54184$ Å) at 100K under a cold nitrogen stream. Structures were solved using direct methods and refined using full-matrix least squares against F^2 with the SHELXL-97 program package. Hydrogen atoms of the organic ligands were added geometrically and the non-hydrogen atoms except for the isordered moieties were refined anisotropically. The crystallographic data has been deposited at the Cambridge Crystallographic Data Center with reference number CCDC 1822327 for complex $\text{Ag}_4\text{N}_2\text{P}_3$. This data can be obtained free of charge from The Cambridge Crystallographic Data Centre via http://www.ccdc.cam.ac.uk/data_request/cif.

Table S1. Crystallographic data for complex $\text{Ag}_4\text{N}_2\text{P}_3$.

Compound	$[\text{Ag}_4(\mu\text{-DMPTP})_2(\text{POP})_3][\text{BF}_4]_2 \cdot 3\text{C}_2\text{H}_5\text{OH}$
Empirical formula	C142H126Ag4N10O6P6B2F8
formula weight	2859.44
crystal system	Triclinic
space group	P-1
a/Å	14.0433 (4)
b/Å	21.6547 (7)
c/Å	22.9726 (6)
α /°	73.403 (2)°
β /°	83.415 (2)°
γ /°	89.935 (2)°
Volume/Å ³	6647.2 (3)
Crystal size [mm ³]	0.15 × 0.14 × 0.14
Z	2
$\rho_{\text{calc}}/\text{g}\cdot\text{cm}^{-3}$	1.438
Index ranges h, k, l	□13/17, □26/26, □27/25
μ/mm^{-1}	5.914
F(000)	2912
$\lambda/\text{Å}$	1.54184
Temperature/K	100
Reflections collected/unique	46034/25147
R_{int}	0.0588
θ range for data collection/°	3.551-70.075
GOF on F^2	1.035
$R_1/\text{WR}_2^{\text{a}}(\text{I}>2\sigma(\text{I}))$	0.0710/0.1900
$R_1/\text{WR}_2^{\text{b}}(\text{all data})$	0.0910/0.2096
CCDC number	1822327

$$^{\text{a}} R_1 = \sum \|F_o\| - |F_c| / \sum \|F_o\|; ^{\text{b}} \text{w}R_2 = [\sum w(F_o^2 - F_c^2)^2 / \sum w(F_o^2)]^{1/2}$$

Table S2. Selected bond distances (Å) and angles (°) of complex $\text{Ag}_4\text{N}_2\text{P}_3$.

Compound	$\text{Ag}_4\text{N}_2\text{P}_3$
----------	-----------------------------------

Distances(Å)	Ag1—N1	2.215 (5)
	Ag1—P1	2.3984 (14)
	Ag1—P2	2.5450 (14)
	Ag2—N6	2.279 (5)
	Ag2—N2	2.298 (5)
	Ag2—P3	2.3639 (14)
	Ag2—N9	2.625 (5)
	Ag3—N3	2.266 (5)
	Ag3—N7	2.284 (5)
	Ag3—P4	2.3502 (13)
	Ag4—N8	2.286 (4)
	Ag4—P5	2.3902 (15)
	Ag4—N10	2.3902 (15)
	Ag4—P6	2.5492 (15)
Angles(°)	N1—Ag1—P1	143.63 (12)
	N1—Ag1—P2	99.72 (12)
	P1—Ag1—P2	113.00 (5)
	N6—Ag2—N2	87.97 (17)
	N6—Ag2—P3	143.61 (11)
	N2—Ag2—P3	143.42 (13)
	N6—Ag2—N9	68.71 (16)
	N2—Ag2—N9	111.44 (16)
	P3—Ag2—N9	113.06 (11)
	N3—Ag3—N7	89.79 (17)
	N3—Ag3—P4	65.51 (16)
	N7—Ag3—P4	124.87 (12)
	N8—Ag4—P5	131.76 (13)
	N8—Ag4—N10	73.95 (17)
	P5—Ag4—N10	124.04 (12)
	N8—Ag4—P6	97.72 (12)
P5—Ag4—P6	97.72 (12)	
N10—Ag4—P6	104.91 (13)	

Fig. S5 ORTEP diagram of $\text{Ag}_4\text{N}_2\text{P}_3$ (the anions, hydrogen atoms and included solvent molecules have been omitted for clarity)

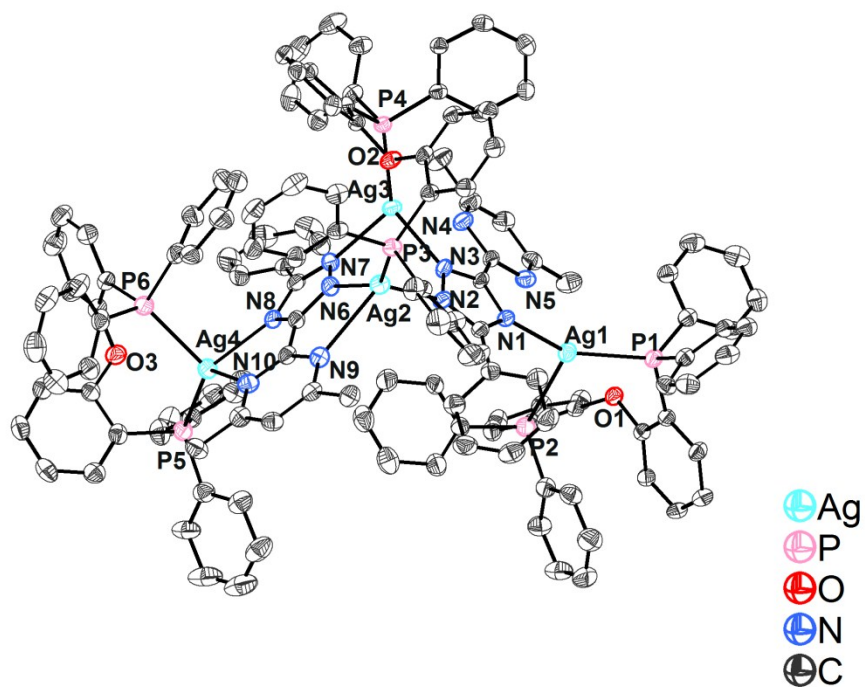


Fig. S6 The structure presentation of $\text{Ag}_4\text{N}_2\text{P}_3$ (Solvent molecules, the anions, H atoms and some phenyl C atoms of the POP ligands are omitted).

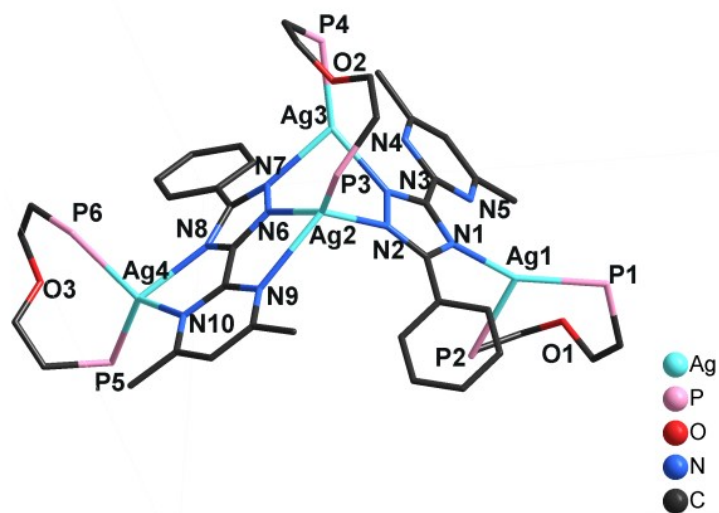
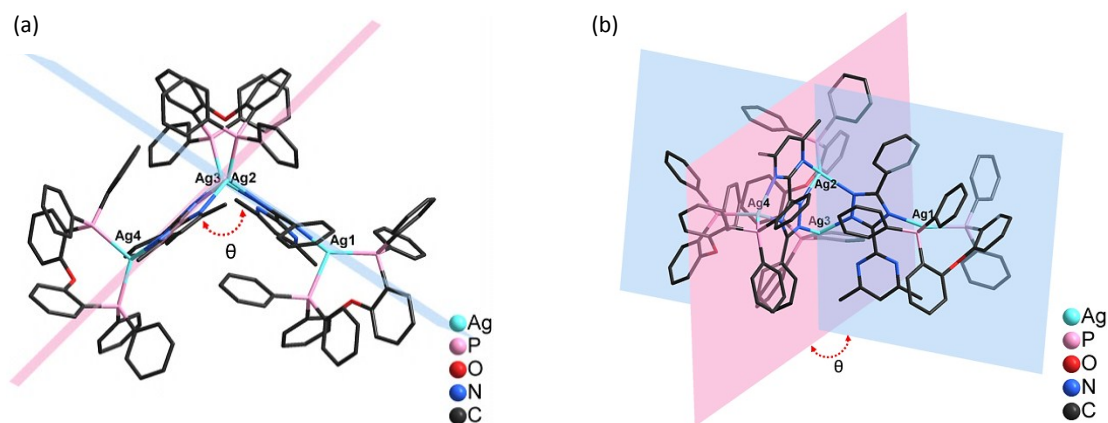


Fig. S7 Schematic representation of the geometrical parameters θ in $\text{Ag}_4\text{N}_2\text{P}_3$ viewed from different sides (Solvent molecules, the anions and H atoms are omitted).



5. Computational studies.

Calculations on the electronic structures of complex $\text{Ag}_4\text{N}_2\text{P}_3$ were carried out by density functional theory (DFT) with Becke's three-parameter B3LYP hybrid functional level. The input data were obtained from the X-ray crystal structure. A "double- ζ " quality basis set consisting of Hay and Wadt's effective core potentials (LANL2DZ) was employed for the Cu atom in which an effective core potential (ECP) replaces the inner core electrons, and the basis set of 6-31G* was used for P, N, C, O and H atoms. Time-dependent DFT (TD-DFT) calculations were performed to determine emission energies at their singlet and triplet excited states using the same functional, basis sets, and crystal model. Natural transition orbitals (NTOs) were computed by applying the unitary transformation that diagonalizes the transition density matrix obtained from TDDFT calculations and represents the electron excitation as a single-particle electron-hole pair. All calculations were carried out using Gaussian 09. The partition orbital composition and electron excitation analysis were calculated by using the Multiwfn 3.4 program.

Table S3. The partition orbital composition analyses for the frontier molecular orbitals of complex $\text{Ag}_4\text{N}_2\text{P}_3$ (based on the X-ray structure).

	Energy (au.)	DMPTP	Ag	POP
HOMO-12	-0.355	47.70%	25.93%	26.36%
HOMO-11	-0.353	47.42%	29.35%	23.22%
HOMO-10	-0.349	16.42%	15.53%	68.04%
HOMO-9	-0.346	5.36%	14.91%	79.73%
HOMO-8	-0.341	4.70%	13.66%	81.64%
HOMO-7	-0.340	5.49%	14.59%	79.92%
HOMO-6	-0.340	1.98%	5.51%	92.51%
HOMO-5	-0.338	26.31%	25.50%	48.19%
HOMO-4	-0.336	56.06%	3.65%	40.29%
HOMO-3	-0.332	82.13%	8.23%	9.64%
HOMO-2	-0.327	28.14%	19.52%	52.34%
HOMO-1	-0.324	8.92%	17.64%	73.44%
HOMO	-0.319	3.50%	18.03%	78.46%
LUMO	-0.167	94.20%	2.13%	3.68%
LUMO+1	-0.165	94.76%	1.97%	3.28%

LUMO+2	-0.163	94.00%	1.83%	4.17%
LUMO+3	-0.161	93.59%	1.70%	4.71%
LUMO+4	-0.145	1.15%	2.39%	96.46%
LUMO+5	-0.144	3.06%	2.06%	94.88%

Fig. S8 The frontier orbitals from HOMO-5 to LUMO+2 of complex $\text{Ag}_4\text{N}_2\text{P}_3$ (based on the X-ray structure).

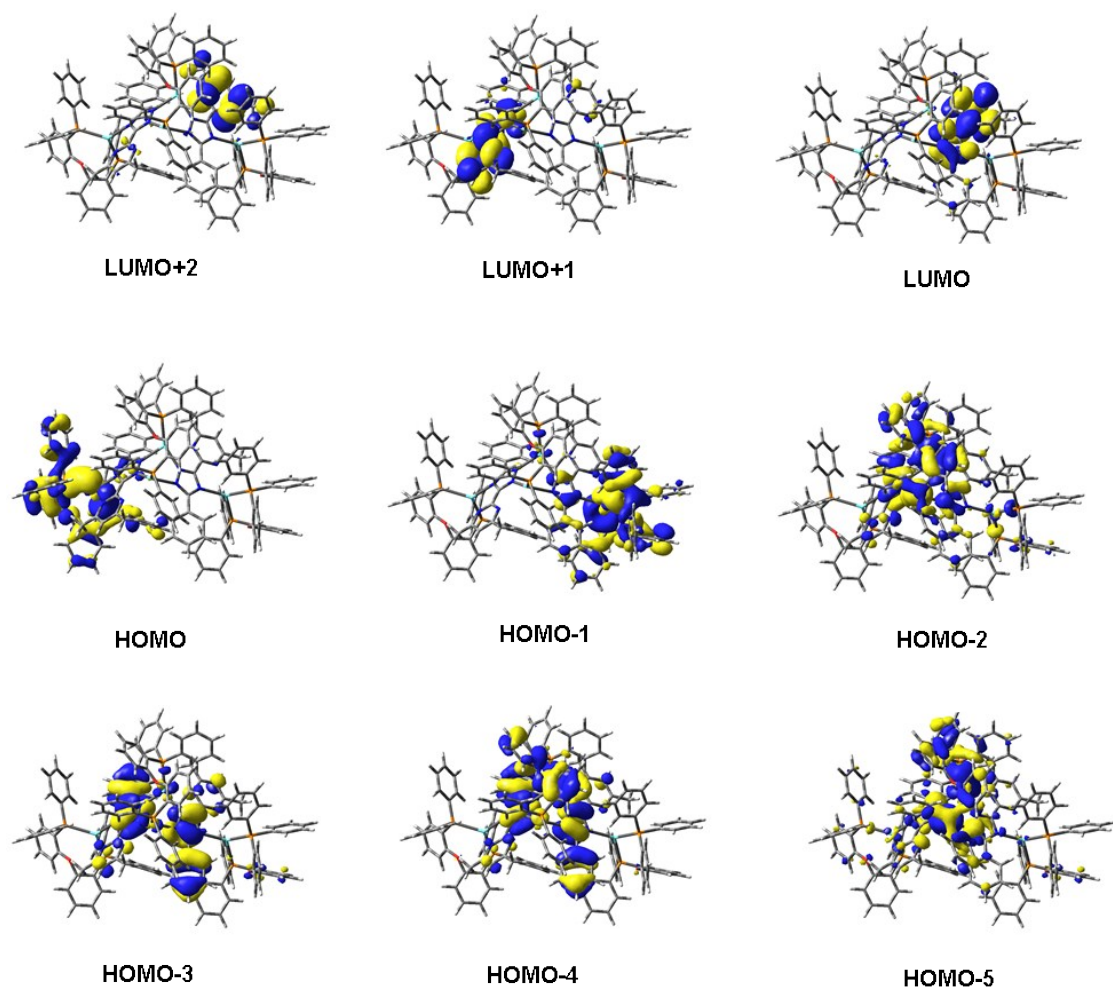
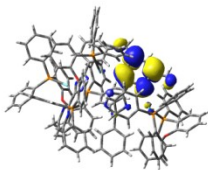
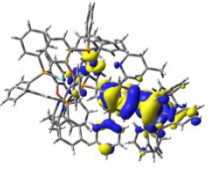
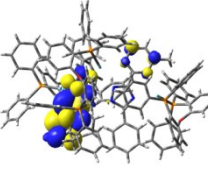
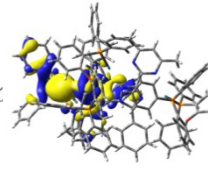
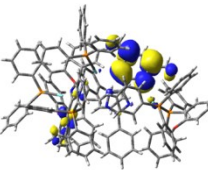
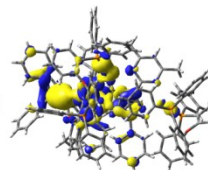
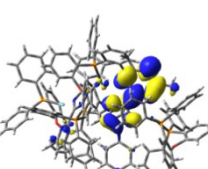
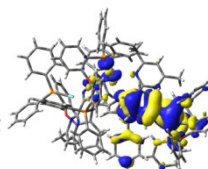
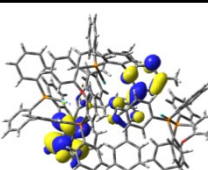
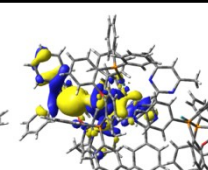
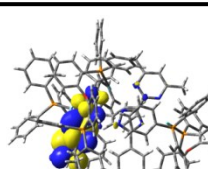
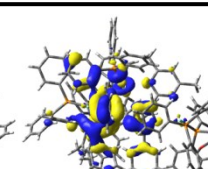
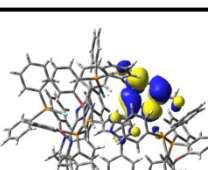
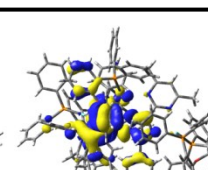
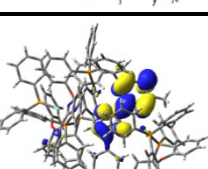
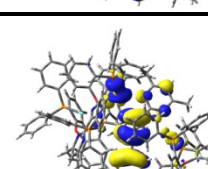
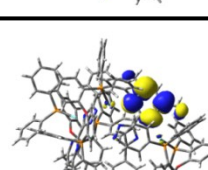
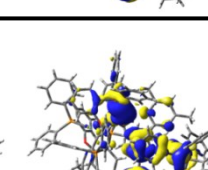


Table S4. Orbital transition analyses for lower-lying transition of complex $\text{Ag}_4\text{N}_2\text{P}_3$ (based on the X-ray structure).

	$\lambda_{cal}(nm)$	f	Main contribution	Electron	Hole	MLCT
S ₁	369.60	0.0232	HOMO-1->LUMO (95%)			19.50%
S ₂	363.47	0.0149	HOMO->LUMO+2 (85%)			
S ₃	361.67	0.0107	HOMO->LUMO (61%)			
S ₅	353.42	0.0135	HOMO-1->LUMO+1 (53%)			
S ₇	344.89	0.0125	HOMO->L+3 (71%)			
S ₉	335.06	0.0141	HOMO-2->L+2 (64%)			
S ₁₀	332.65	0.0023	HOMO-3->LUMO (76%)			
T ₁	405.58	0	HOMO-1->LUMO+1 (22%)			10.37%
T ₂	379.32	0	HOMO-1->LUMO (60%)			

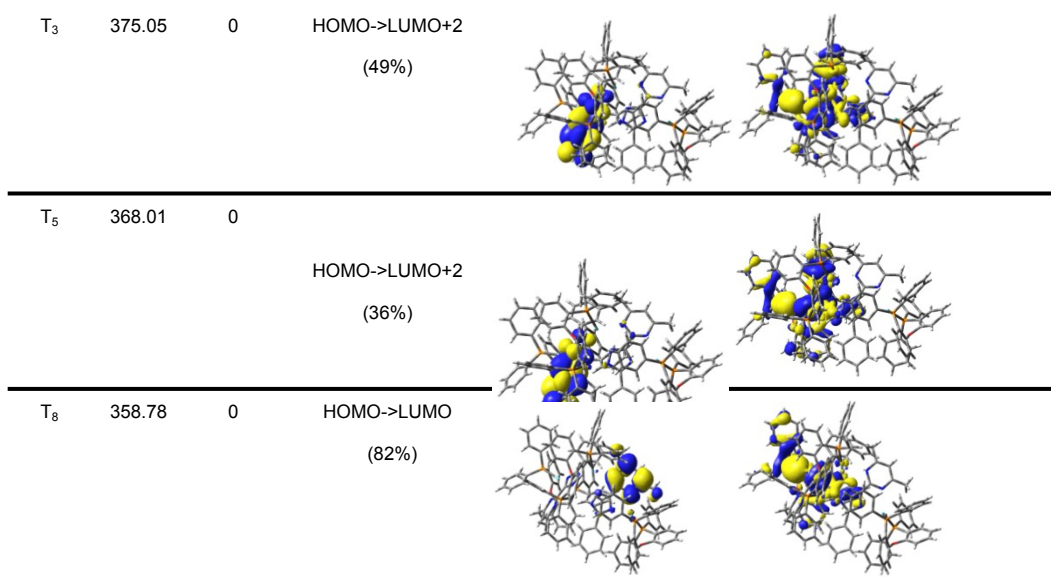


Table S5. The partition composition analyses for the lower-lying excited states of complex Ag₄N₂P₃ (based on the X-ray structure).

		Ag	DMPTP	POP
S ₁	hole	22.06%	13.65%	64.29%
	electron	2.57%	93.49%	3.94%
	difference	19.50%	-79.84%	60.34%
S ₂	hole	24.86%	7.41%	67.72%
	electron	2.89%	92.50%	4.62%
	difference	21.98%	-85.08%	63.10%
T ₁	hole	13.24%	69.79%	16.97%
	electron	2.87%	91.46%	5.67%
	difference	10.37%	-21.67%	11.30%
T ₂	hole	22.37%	34.16%	43.47%
	electron	2.65%	93.40%	3.95%
	difference	19.73%	-59.25%	39.52%